Bulletin of the Seismological Society of America, Vol. 105, No. 6, pp. 3024–3035, December 2015, doi: 10.1785/0120150163

Inversion for the Composite Moment Tensor

by Václav Vavryčuk

Abstract The composite moment tensor is defined in analogy to the composite focal mechanism as the averaged representative seismic moment tensor characteristic for a focal area under study. In contrast to the composite focal mechanism, which provides information on shear faulting, the composite moment tensor can provide additional information on nonshear rupture mode and on physical conditions along the fault. The composite moment tensor is calculated by a joint inversion of multiple earthquakes associated with the same fault system and displaying a similar focal mechanism. The method utilizes amplitudes of *P* and/or *S* waves or full waveforms. Because the inversion is linear, it is fast and applicable to datasets of many earthquakes. The method is particularly suitable for the analysis of microseismicity, earthquake swarms, or aftershock sequences, where observations of multiple earthquakes are available. The composite moment tensor can be retrieved even when the station configuration or data quality prevent inversion for the full moment tensors of individual earthquakes.

Introduction

The seismic moment tensor is a fundamental quantity that characterizes physical processes at the earthquake source. The double-couple (DC) component of the moment tensor is produced by shear faulting and provides information on the fault orientation and the direction of slip along the fault. The non-double-couple (non-DC) components are produced by tensile faulting, cavity collapses, irregularities of the fault geometry, or seismic anisotropy in the focal area (Julian *et al.*, 1998; Miller *et al.*, 1998; Vavryčuk, 2002, 2011b, 2015). The determination of moment tensors is, however, a demanding procedure that requires observations from many stations, good station coverage of the focal zone, accurate locations, and accurate knowledge of the velocity model (Šílený, 2009; Zahradník and Custodio, 2012; Stierle, Bohnhoff, and Vavryčuk, 2014; Stierle, Vavryčuk, *et al.*, 2014).

The number of stations used in the inversion is a critical parameter in determining accurate moment tensors. If the seismicity is observed at a few stations only, the accuracy of the moment tensors is worse or the moment tensors cannot be determined at all. This difficulty can be overcome by combining different types of data in the inversion (Fojtíková and Zahradník, 2014; Vavryčuk and Kim, 2014) or by combining data of many earthquakes occurring at the same focal area and associated with the same fault system. So far, the latter approach has been developed and applied to determining the so-called composite focal mechanisms using *P*-wave polarities observed for a family of multiple events. If an intense seismic activity is observed in some area (e.g., frequently repeating earthquakes, aftershocks or earthquake swarms), the earthquakes can be classified using cross correlation of waveforms and then grouped into multiplets (Rubin *et al.*, 1998; Li *et al.*, 2011; Myhill *et al.*, 2011; Schaff and Richards, 2011). Instead of inverting for focal mechanisms of individual earthquakes, the *P*-wave polarities observed for the whole multiplet can jointly be inverted for a common focal mechanism. In this way, variations of individual focal mechanisms due to small-scale inhomogeneities or numerical errors are suppressed and only an averaged focal mechanism is retrieved. This method proved to be useful and produced representative focal mechanisms in various seismoactive areas (Got *et al.*, 1994; Ferreira *et al.*, 1998; Rutledge *et al.*, 1998; Rutledge and Phillips, 2003; Scarfì *et al.*, 2003; Shearer *et al.*, 2003; Sato *et al.*, 2004; Godano *et al.*, 2014).

In this article, we generalize the idea of the composite focal mechanism and introduce the composite moment tensor as the representative common moment tensor characteristic for earthquakes in the same focal area occurring on the same fault. Introducing the composite moment tensor is important for several reasons. First, the composite moment tensors provide more information on rupture modes and physical conditions at the focal zone than do the composite focal mechanisms. Second, the composite moment tensor is an overall quantity less prone to numerical errors and to deviations due to small-scale fault irregularities or material and stress inhomogeneities in the focal area. Third, the composite moment tensor represents mathematically an average of a set of noisy moment tensors.

The determination of the composite moment tensor is based on a joint inversion for one common moment tensor using amplitudes of *P* and/or *S* waves or using full waveforms observed at a limited number of stations but for multiple earthquakes. The inversion is linear and yields the composite moment tensor and the scale factors of individual multiple events. The robustness of the method is numerically tested. Finally, the method is applied to microearthquakes that occurred during the 2008 earthquake swarm in West Bohemia, Czech Republic.

Method

The standard moment tensor inversion for one individual event is based on the following equation:

$$\mathbf{G}\,\mathbf{m} = \mathbf{u}, \tag{1}$$

in which $\mathbf{G}$ is the $K \times 6$ matrix of the spatial derivatives of the Green's function,

$$\mathbf{G} = \begin{bmatrix} G_{11} & G_{12} & G_{13} & G_{14} & G_{15} & G_{16} \\ G_{21} & G_{22} & G_{23} & G_{24} & G_{25} & G_{26} \\ \cdots & \cdots & \cdots & \cdots & \cdots & \cdots \\ G_{K1} & G_{K2} & G_{K3} & G_{K4} & G_{K5} & G_{K6} \end{bmatrix}, \tag{2}$$

$\mathbf{m}$ is the vector composed of six components of moment tensor $\mathbf{M}$,

$$\mathbf{m} = [\,M_{11} \quad M_{22} \quad M_{33} \quad M_{23} \quad M_{13} \quad M_{12}\,]^T, \tag{3}$$

and $\mathbf{u}$ is the vector of displacement amplitudes or of full displacement waveforms observed at K sensors. Quantities G_{ki} are the components of the Green's function matrix for the kth sensor:

$$\begin{aligned} &G_{k1} = G_{k1},_1\,, G_{k2} = G_{k2},_2\, G_{k3} = G_{k3},_3\,, \\ &G_{k4} = G_{k2},_3 + G_{k3},_2\,, G_{k5} = G_{k1},_3 + G_{k3},_1\,, \\ &G_{k6} = G_{k1},_2 + G_{k2},_1\,, \end{aligned} \tag{4}$$

in which $G_{kl},_m = \frac{\partial G_{kl}}{\partial \xi_m}$ is the spatial derivative of the Green's function for the kth sensor produced by the force along the l axis and oriented along the sensor direction. If we invert amplitudes of the P and/or S waves, the components of the Green's function G_{ki} are scalar quantities. If we invert the full waveforms, the components G_{ki} are vectors of amplitudes dependent on time.

For two events, we get:

$$\mathbf{G}^{(1)}\mathbf{m}^{(1)} = \mathbf{u}^{(1)}, \tag{5}$$

and

$$\mathbf{G}^{(2)}\mathbf{m}^{(2)} = \mathbf{u}^{(2)}. \tag{6}$$

If the two events have the same moment tensor except for scaling, then

$$\mathbf{m}^{(2)} = \mathbf{m}^{(1)}/C^{(2)}, \tag{7}$$

in which $C^{(2)} = M^{(1)}/M^{(2)}$ is the ratio between the scalar moments of the first and second event, and we can write from equation (6)

$$\mathbf{G}^{(2)}\mathbf{m}^{(1)} = C^{(2)}\mathbf{u}^{(2)}. \tag{8}$$

Combining equations (5) and (8), we obtain a system of equations for moment vector $\mathbf{m}^{(1)}$ and scale factor $C^{(2)}$:

$$\begin{bmatrix} \mathbf{G}^{(1)} & \mathbf{0} \\ \mathbf{G}^{(2)} & -\mathbf{U}^{(2)} \end{bmatrix} \begin{bmatrix} \mathbf{m}^{(1)} \\ C^{(2)} \end{bmatrix} = \begin{bmatrix} \mathbf{u}^{(1)} \\ 0 \end{bmatrix}. \tag{9}$$

Equation (9) can readily be generalized to N events:

$$\begin{bmatrix} \mathbf{G}^{(1)} & \mathbf{0} & \mathbf{0} & \cdots & \mathbf{0} \\ \mathbf{G}^{(2)} & -\mathbf{u}^{(2)} & \mathbf{0} & \cdots & \mathbf{0} \\ \mathbf{G}^{(3)} & \mathbf{0} & -\mathbf{u}^{(3)} & \cdots & \mathbf{0} \\ \vdots & \vdots & \vdots & \ddots & \vdots \\ \mathbf{G}^{(N)} & \mathbf{0} & \mathbf{0} & \cdots & -\mathbf{u}^{(N)} \end{bmatrix} \begin{bmatrix} \mathbf{m}^{(1)} \\ C^{(2)} \\ C^{(3)} \\ \vdots \\ C^{(N)} \end{bmatrix} = \begin{bmatrix} \mathbf{u}^{(1)} \\ \mathbf{0} \\ \mathbf{0} \\ \vdots \\ \mathbf{0} \end{bmatrix}, \tag{10}$$

in which $C^{(n)}$ is the scale factor of the nth event and $\mathbf{u}^{(n)}$ is the vector composed of displacement amplitudes or waveforms $u_k^{(n)}$ of the nth event observed at the kth sensor, such that

$$\mathbf{u}^{(n)} = [\,u_1^{(n)} \quad u_2^{(n)} \quad u_3^{(n)} \quad \ldots \quad u_K^{(n)}\,]^T. \tag{11}$$

Inverting equation (10) using the generalized linear inversion (Menke, 1989), we get vector $\mathbf{m}^{(1)}$ and scale factors $C^{(n)}$, $n = 2, \ldots, N$. From vector $\mathbf{m}^{(1)}$, we get tensor $\mathbf{M}^{(1)}$ using equation (3). The composite moment vector $\mathbf{m}$ and moment tensor $\mathbf{M}$ are obtained by normalizing $\mathbf{m}^{(1)}$ and $\mathbf{M}^{(1)}$ by scalar moment $M^{(1)}$. Hence, the norm of the composite moment tensor $\mathbf{M}$ equals 1.

Equation (10) can be modified by considering scale factor $C^{(1)}$ of the first event as unknown and by imposing another equation for the whole set of scale factors. For example, we can assume the mean value of the scale factors to be 1. Such equations are more symmetric, and no event is considered as preferential in the inversion. It is also advantageous to scale the amplitudes or waveforms of individual events before the inversion. In this case, the weight of individual events will be similar in the inversion. The weight of the events can also be controlled by the quality of waveforms or amplitude readings.

The accuracy of the moment vector $\mathbf{m}$ and scale factors $C^{(n)}$ can be improved further by iterations. Each iteration consists of two steps. First, knowing scale factors $C^{(n)}$, we normalize observations of the individual events and invert the observations of all events just for $\mathbf{m}$. Second, the composite moment vector $\mathbf{m}$ is fixed in the inversion, and new scale factors are calculated. The success of the iterative inversion can be measured by the convergence of $\mathbf{m}$ and $C^{(n)}$. No convergence of $\mathbf{m}$ and $C^{(n)}$ indicates that the input data are either too noisy or the scatter of the moment tensors of individual events is too high for calculating a reliable composite moment tensor.

For illustration, if amplitudes of 10 events recorded at one sensor are inverted for the composite moment tensor, the inversion is based on solving a system of 10 equations for 15 unknowns (six components of $\mathbf{M}$ and nine scaling factors), which is an underdetermined problem. However, if amplitudes of 10 events recorded at two sensors are inverted for the composite moment tensor, a system of 20 equations is solved for 15 unknowns, which is an overdetermined problem. Hence, the composite solution and the scalar moments

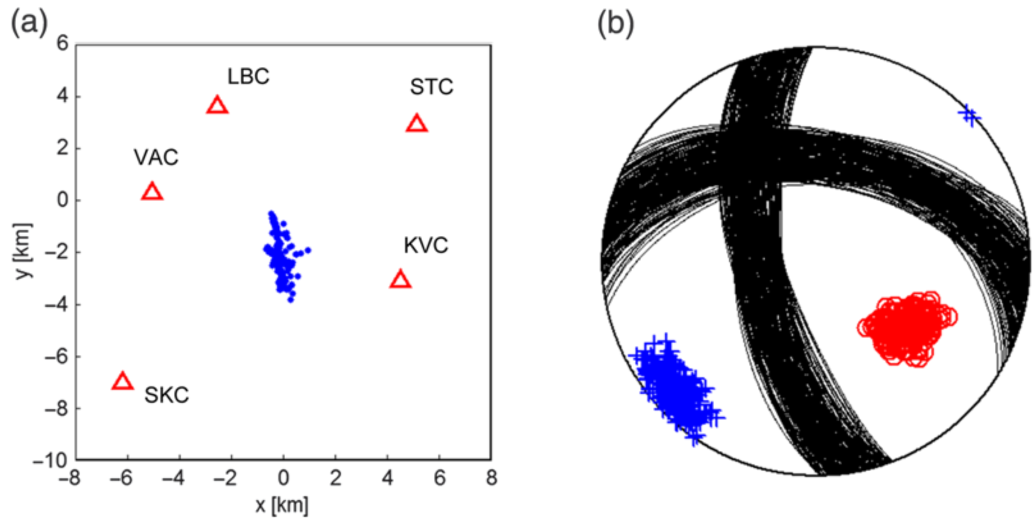

Figure 1. (a) The locations of stations (red triangles) with the distribution of epicenters (blue dots) and (b) the focal mechanisms of 200 earthquakes used in the synthetic tests. Red circles mark the P axes, and blue plus signs mark the T axes. The lower hemisphere equal-area projection is used.

can be retrieved from observations of two one-component stations only. The events can be of different magnitudes but they should have a similar focal mechanism. Obviously, using more stations and the more events in the inversion will yield a more reliable and more accurate composite solution.

In case of the waveform inversion for the composite moment tensor, the situation is even more favorable than for the amplitude inversion. Because amplitude at each time instant represents one equation in the inversion, the problem is always well overdetermined. In principle, the moment tensor can be retrieved by inverting a full waveform recorded at one station only, provided the earthquake location and the velocity model are known with a high accuracy. Because this is not usually the case and the velocity model is often not well known, waveforms of more stations must be used to stabilize the inversion and to obtain a reliable moment tensor. Calculating the composite moment tensor has exactly the same effect. Instead of inverting several similar individual moment tensors using waveforms observed at a few stations only, we invert for one composite moment tensor using many observed waveforms. For example, instead of inverting for moment tensors of five events recorded at three stations, we invert for one composite moment tensor using recordings at 15 stations. Obviously, this approach is advantageous only if the events have different locations. If the hypocenters are close or identical, the observations of different events do not provide additional independent information.

Finally, let us summarize conditions which should be satisfied in the composite moment tensor inversion. As for the standard moment tensor inversion, the accuracy of the joint inversion increases if (1) sensors ensure good coverage of the focal sphere, (2) amplitudes or waveforms of events have a good signal-to-noise ratio, (3) the velocity model is well known, and (4) event locations are accurate. In addition, a dataset of at least several events with a similar focal mechanism is required, and the events should have different locations for the inversion to be stable.

Numerical Tests

We perform synthetic tests illustrating the robustness of the proposed inversion scheme. We use several station configurations, focal mechanisms with a variable level of their similarity, and input data contaminated by various levels of noise. Depths of events, the velocity model, and the station configurations are used to mimic observations of microearthquakes in the West Bohemia region used as an example in the next section. The hypocenter depth is in the range of 7–11 km, a 1D layered velocity model is used, and the epicentral distance of stations is less than 10 km. We determined the composite moment tensors using vertical components of amplitudes of the direct *P*-wave recorded alternatively at three, four, or five stations (see Fig. 1a). We inverted 100 or 200 shear earthquakes with similar focal mechanisms with strikes, dips, and rakes randomly generated and uniformly distributed in the intervals of $169° \pm 10°$, $68° \pm 10°$, and $-44° \pm 10°$, respectively (see Fig. 1b). This focal mechanism is typical for the activity in West Bohemia and represents the principal focal mechanism in the region (Vavryčuk, 2011a). The other principal focal mechanism in the region has strike, dip, and rake of 304°, 66°, and −137°. This focal mechanism is less frequent than the previous one and will be used in datasets containing some portion of events with a dissimilar focal mechanism. The Green's function needed for calculating synthetic amplitudes and subsequently for inverting for the composite moment tensor were calculated for a layered isotropic velocity model using the ray method (Červený, 2001).

Sensitivity Tests

Figure 2 shows the results of the inversion for the composite moment tensor using a dataset of 200 focal mech-

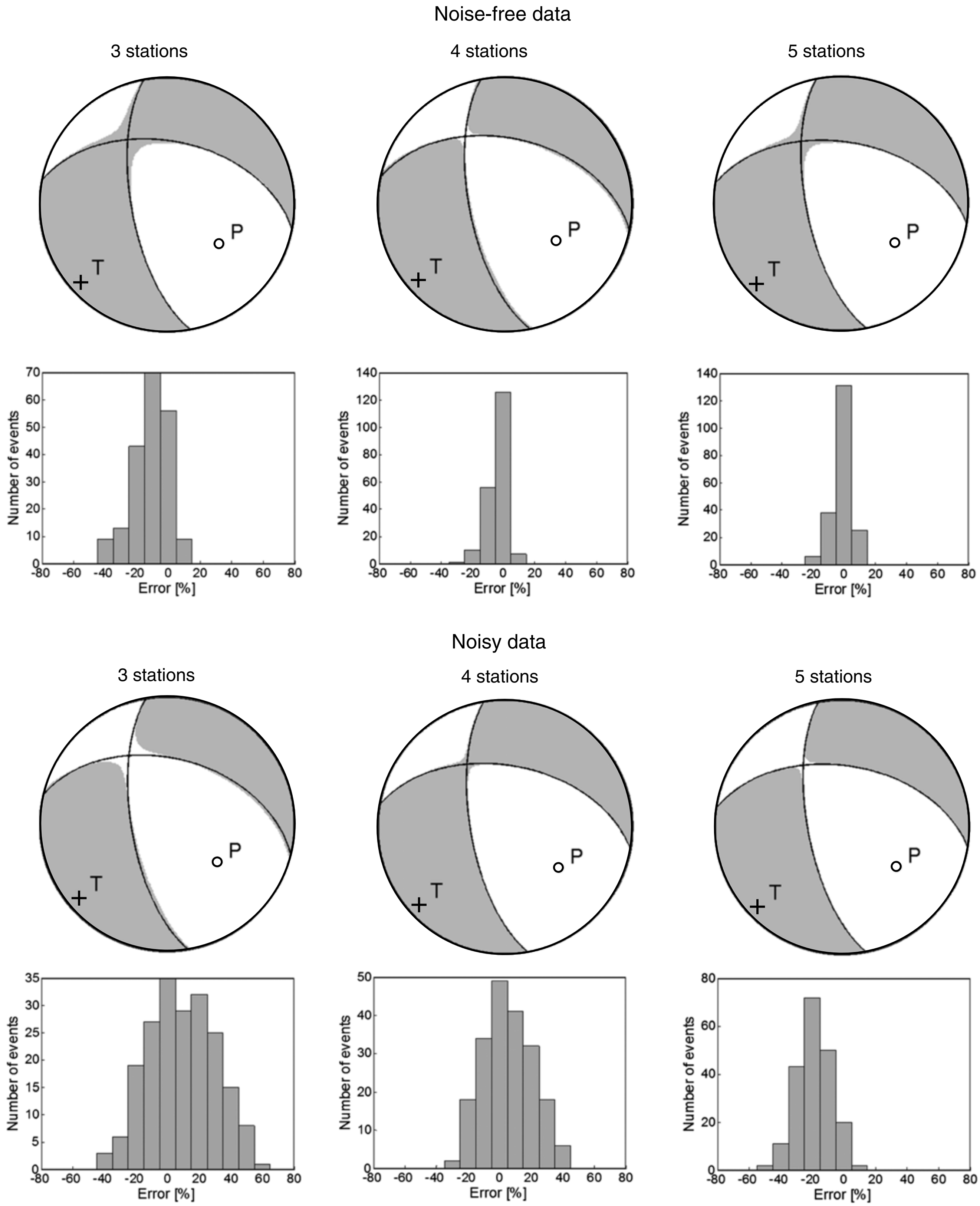

Figure 2. The composite moment tensor inversion of a synthetic dataset with 200 earthquakes. The results of the inversion are shown for noise-free amplitudes (upper plots) and for noisy amplitudes (lower plots) with the noise level up to $\pm 30\%$ of the maximum *P*-wave amplitude at the respective station. The following station configurations were used: three stations, LBC, KVC, and SKC; four stations, LBC, KVC, SKC, and VAC; and five stations, LBC, KVC, SKC, VAC, and STC. The figure shows the composite focal mechanisms and histograms of errors of the scale factors of individual events. The errors of the scale factors are calculated as the relative differences between the true and retrieved scale factors.

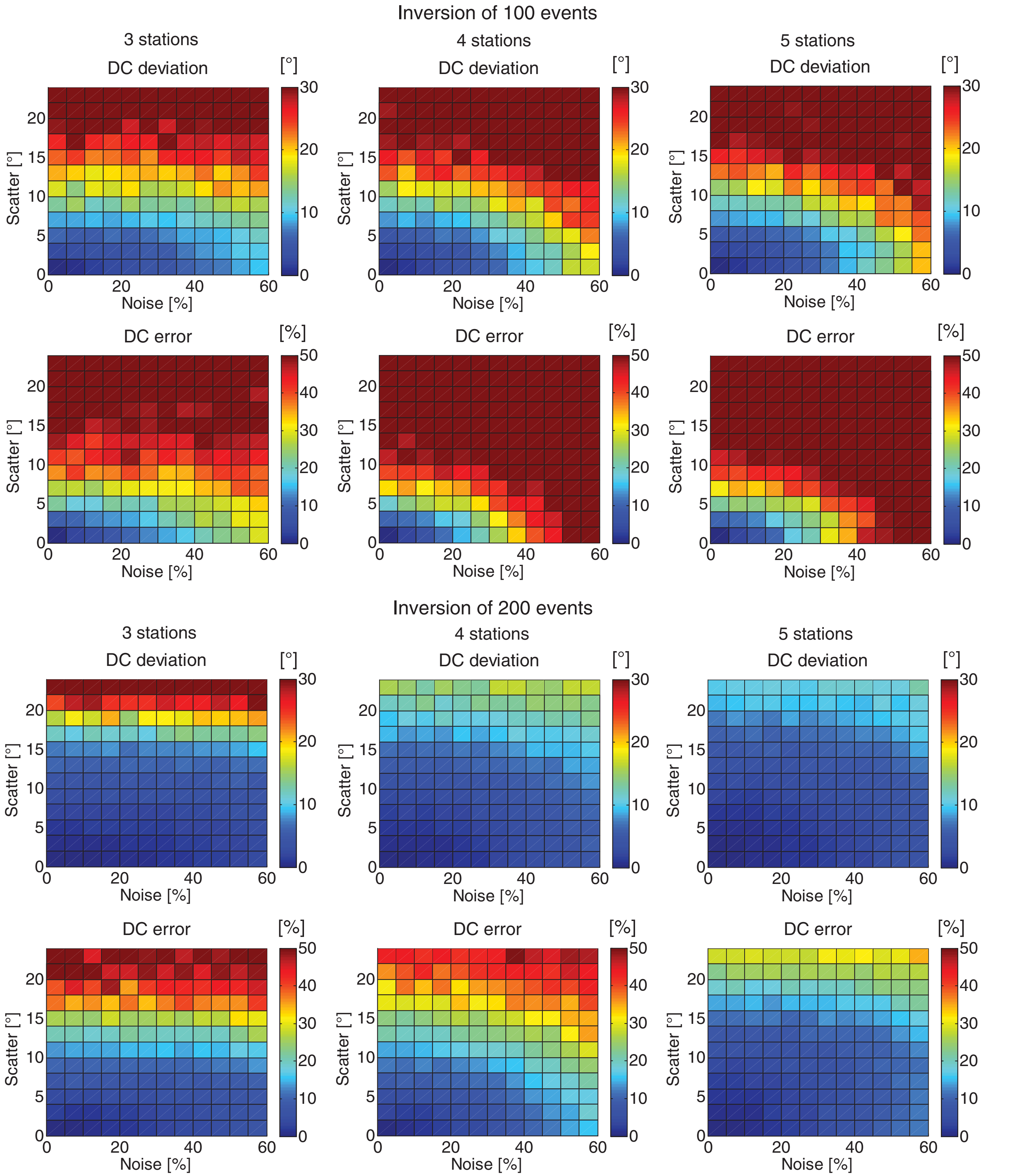

Figure 3. Statistical test of the composite moment tensor inversion. The errors in the orientation of the composite double-couple (DC) mechanisms (DC deviation) and the errors in the percentage of the DC component (DC error) are shown as a function of noise in the *P*-wave amplitudes and the scatter of focal mechanisms in the input dataset of events. The percentage of the DC and non-DC components was calculated according to formulas of Vavryčuk (2001). The errors are color coded and calculated as an average of 100 random realizations of noise in amplitudes and scatter of focal mechanisms.

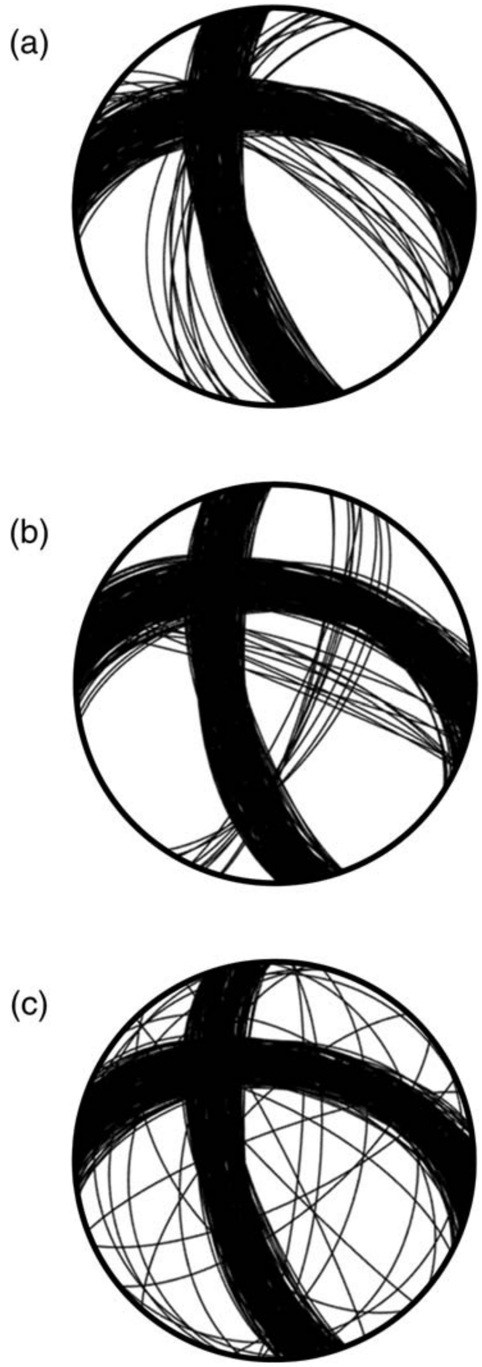

Figure 4. Datasets of 200 similar events and 10 outliers. (a) Dataset A, outliers have a mean focal mechanism with strike, dip, and rake of 304°, 66°, and −137°; (b) dataset B, outliers have a mean focal mechanism with strike, dip, and rake of 25°, 70°, and 10°; and (c) dataset C, outliers have random shear focal mechanisms.

anisms for three different station configurations (see Fig. 1b). The inversion was performed for noise-free and noisy *P*-wave amplitudes. The noise was random with a uniform distribution, and its level was up to ±30% of the *P*-wave amplitude at the respective station. The results indicate that the inversion works well for all three station configurations. The DC component of the composite moment tensor fits the true synthetic focal mechanism quite well. The inversion generated also minor non-DC components, causing the shaded areas in the beach balls to not follow the nodal lines exactly. As expected, the noisy input data produce results with a lower accuracy. Similarly, a decreasing number of stations produces less accurate results. Nevertheless, the tests proved that the method works well and can provide useful information on the composite focal mechanism and scale factors even in such unfavorable cases when only *P*-wave amplitudes from three one-component stations are available.

In order to better assess the accuracy of the method, we performed additional numerical tests. We focused on analyzing the sensitivity of the composite moment tensor to (1) the scatter of the focal mechanisms in the inversion and (2) the level of noise in input *P*-wave amplitudes. To obtain statistically relevant results, the random noise and random distribution of focal mechanisms were generated repeatedly 100 times, and the results of the inversion were averaged. Figure 3 shows the errors in the composite focal mechanism and in the DC percentage of the retrieved composite moment tensor for the datasets of 100 and 200 events. The errors in the mechanism are quantified by the DC deviation δ, calculated as the average of deviations of fault normals $\mathbf{n}^{(i)}$ and slip directions $\mathbf{s}^{(i)}$ of the retrieved composite focal mechanisms from fault normal $\mathbf{n}$ and slip direction $\mathbf{s}$ of the true composite focal mechanism:

$$\delta = \frac{1}{2N}\left(\sum_{i=1}^{N} \mathrm{a}\cos(\mathbf{n}^{(i)} \cdot \mathbf{n}) + \sum_{i=1}^{N} \mathrm{a}\cos(\mathbf{s}^{(i)} \cdot \mathbf{s})\right), \quad (12)$$

in which N is the number of multiple events and the dot is the scalar product.

The inversion of 100 events yields reasonable results with the error in the composite focal mechanism less than 10° only for noise in amplitudes less than 30% and for a scatter in input focal mechanisms less than 6°. Similar conditions apply to errors in the DC percentage less than 20%. By contrast, the inversion of 200 events works significantly better than that of 100 events. It is less sensitive to the amplitude errors as well as to the scatter in the focal mechanisms. The inversion yields errors in the composite focal mechanism less than 10° for noise in amplitudes less than 50%–60% and for a scatter in input focal mechanisms less than 10°–15°. The accuracy further increases with increasing number of stations.

Procedure for Removing Outliers

In the previous tests, we assumed that the focal mechanisms of the analyzed earthquakes were similar. However, it might happen that some earthquakes have a focal mechanism associated with another active fault or fault system. Apparently, the presence of such "outliers" in the dataset violates the basic assumptions of the method and leads to lowering the accuracy of the composite moment tensor. We analyze such ill-posed cases and check whether the performance of the inversion can

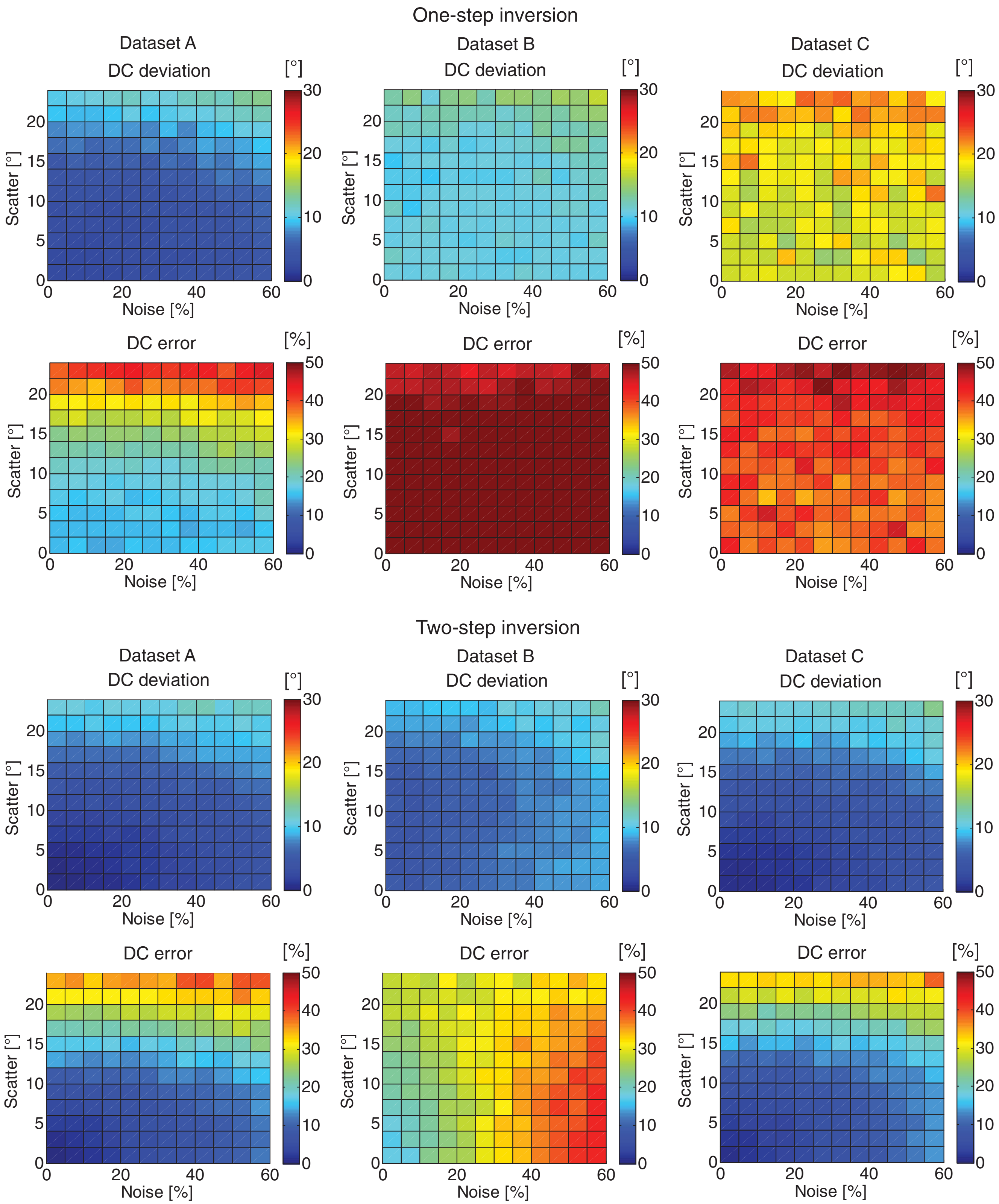

Figure 5. Statistical test of the composite moment tensor inversion: datasets with outliers. Datasets contain 200 events with similar focal mechanisms and 10 outliers (see Fig. 4). One-step inversion assumes all events in the inversion have a similar focal mechanism; in two-step inversion, the 15 events with the highest root mean square (rms) are assumed to be outliers and excluded in the second step. For meaning of the quantities, see the caption of Figure 3.

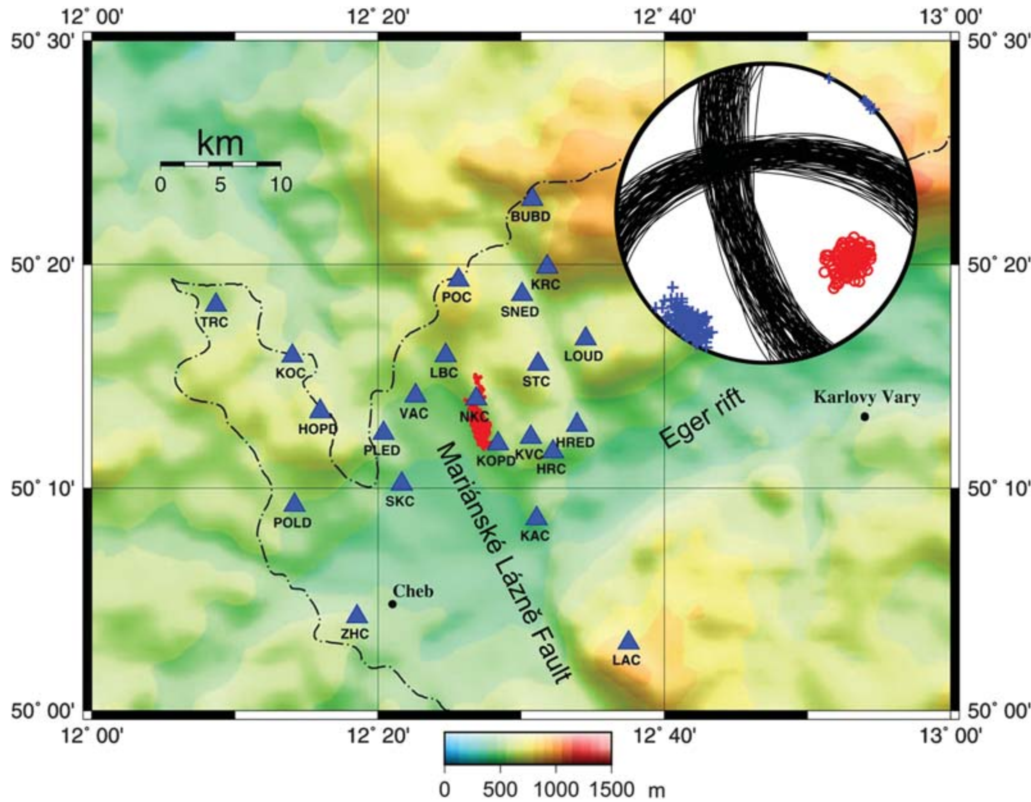

Figure 6. Topographic map of the West Bohemia region. The epicenters of the 2008 swarm microearthquakes are marked by the red dots, and the West Bohemia Network (WEBNET) stations are marked by the blue triangles. The inset shows the focal mechanisms of 111 selected earthquakes under study. The red circles mark the P axes, and the blue plus signs mark the T axes.

be improved when some criteria for identifying and removing the outliers during the inversion are applied.

We modify the dataset of 200 events with similar focal mechanisms by including an additional 10 events with a different focal mechanism. We consider three alternative datasets, A, B, and C, which differ in the focal mechanisms of outliers (see Fig. 4). The outliers of dataset A have focal mechanisms close to the other principal focal mechanism in the West Bohemia region with strike, dip, and rake of $304° \pm 10°$, $66° \pm 10°$, and $-137° \pm 10°$, respectively. The outliers of dataset B have focal mechanisms with strike, dip, and rake of $25° \pm 10°$, $70° \pm 10°$, and $10° \pm 10°$. These focal mechanisms are quite different from those of the 200 events. Finally, the outliers of dataset C have focal mechanisms that are fully random. Outliers in all three datasets have shear focal mechanisms. The three datasets are used for testing the sensitivity of the inversion for the composite moment tensor when the datasets are contaminated by outliers of various levels of dissimilarity.

The inversion is performed in two steps. First, the standard procedure is applied assuming that all focal mechanisms are similar. Second, the root-mean-square (rms) misfit of synthetic amplitudes and those predicted for the retrieved composite moment tensor are evaluated for individual events, and the events with the highest misfit are discarded. To mimic a real situation in which the number of outliers is not exactly known, we discarded a slightly higher number of low-fit events (10 instead of 15). After removing these events, the inversion for the composite moment tensor is run again. The sensitivity tests of the resultant composite moment tensor are performed for the configuration of five stations (see Fig. 1a) and in a similar way as for the dataset with no outliers (see Fig. 3). The results of the one-step and two-step inversions, are shown in Figure 5.

The tests confirm that outliers decrease the accuracy of the composite moment tensor. The most critical parameter is the error in the DC percentage. The DC error is about 10% for a dataset with no outliers for similar focal mechanisms with a scatter up to 10°–15° (Fig. 3, plot for 200 events and five stations). However, the DC error increases to about 20%, 50%, and 40% for datasets A, B, and C, respectively (Fig. 5, plots for one-step inversion). In particular, if outliers have a consistent but very different focal mechanism (dataset B), the standard inversion fails. Also randomly oriented outliers distort the orientation as well as the DC percentage of the composite moment tensor.

The two-step inversion performs much better than the one-step inversion (see Fig. 5, lower plots). The DC deviation is retrieved for all three datasets with almost the same accuracy as for the dataset with no outliers. The DC errors for datasets A and C are also similar to those for the no-outlier dataset. Hence, the two-step inversion suppresses the influence of outliers that have slightly deviating consistent mechanisms (data-

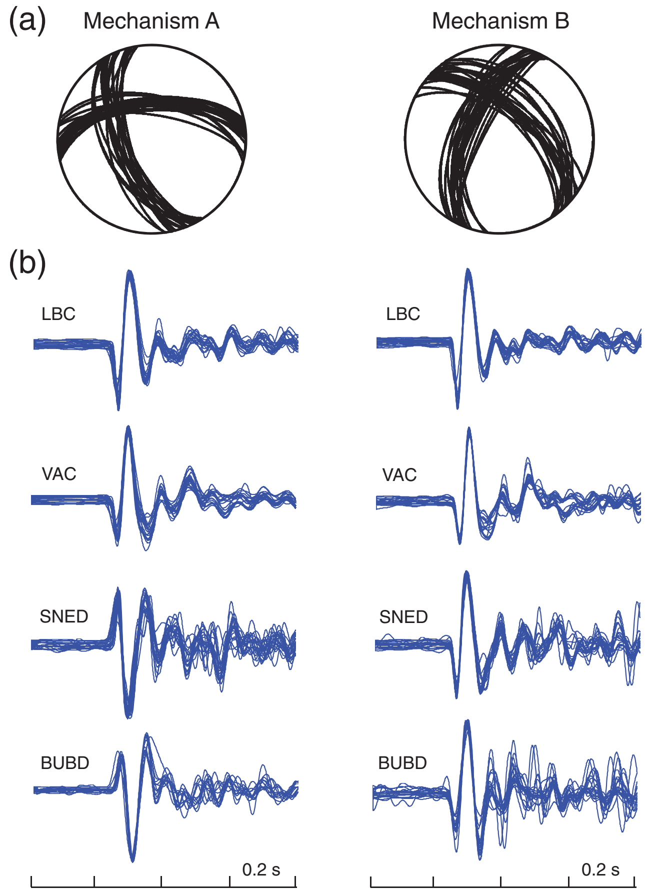

Figure 7. *P* waveforms of two multiplets formed by 20 earthquakes with similar focal mechanisms. The magnitudes of earthquakes range from 0.6 to 3.5. The velocity records are normalized and filtered using a band-pass Butterworth filter in the range of 1–10 Hz. Mechanisms A and B are the principal mechanisms observed in the West Bohemia area (Vavryčuk, 2011a). The focal mechanisms of individual earthquakes are calculated using the moment tensor inversion of *P*-wave amplitudes at a minimum of 18 stations. Note the reverse polarities of the two multiplets at the SNED and BUBD stations.

set A) or fully random mechanisms (dataset C). However, the DC errors for dataset B remain high, as in the one-step inversion. Hence, the DC percentage of the composite moment tensor is unreliable if outliers have consistent but quite dissimilar mechanisms than the predominant one.

Application to the 2008 West Bohemia Earthquake Swarm

The West Bohemia region is a seismically active area with a frequent occurrence of earthquake swarms (Fischer *et al.*, 2010, 2014; Čermáková and Horálek, 2015). One of the most recent and prominent swarms was recorded in October 2008. The 2008 swarm lasted for four weeks and included 25,000 microearthquakes. The strongest event reached a magnitude of 3.7. The hypocenters were located at depths of 7.5–11 km (Bouchaala *et al.*, 2013; Vavryčuk *et al.*, 2013). The seismic activity in the area is connected to young Quaternary volcanism manifested by mineral water springs with high carbon dioxide content (Babuška *et al.*, 2007; Fischer *et al.*, 2014). The seismicity is monitored by 22 short-period seismic stations of the West Bohemia Network (WEBNET), with the sampling frequency of 250 Hz (see Fig. 6). Because the focal area is quite small, the waveforms of earthquakes are very similar and can be grouped into multiplets according to their focal mechanism (see Fig. 7). The events recorded in 2008 can be attributed to two principal focal mechanisms. The majority of the events are the left-lateral strike slips with a strike of 169°. A small portion of events display a mechanism of the right-lateral strike slip with a strike of 304° (Vavryčuk, 2011a).

The composite moment tensor inversion is illustrated on a dataset of 111 microearthquakes with the left-lateral strike-slip focal mechanisms. First, the moment tensors were calculated using the standard inversion of *P*-wave amplitudes measured at vertical records of the WEBNET stations. The minimum number of stations used was 18. The moment tensors are predominantly double couples and have similar focal mechanisms. The non-DC parts are mostly less than 30% and consist of negative isotropic (ISO) and compensated linear vector dipole (CLVD) components (for definition, see Vavryčuk, 2015). The composite moment tensor inversion is run for amplitudes measured at 4, 6, 8, 10, and 18 stations. The results are compared with the accurate moment tensors.

As indicated in Figure 8 and Table 1, the composite moment tensor determined using four stations reproduces the accurate focal mechanisms quite well. The signs of the ISO and CLVD components are reversed, but their values are small. The fit of the composite solution with the accurate moment tensors is improving with increasing number of stations. The P/T axes of the composite solution calculated from 8 or 10 stations lie in the center of the clusters of the P/T axes of the accurate solutions. The position of the composite solution in the CLVD-ISO source type plot is inside the cluster of the accurate moment tensors.

Discussion and Conclusions

Calculating the composite moment tensor of multiple earthquakes might be a powerful tool for studying stress conditions, fracture mode, and other physical conditions at the focal zone. The composite moment tensor is a representative overall quantity describing processes in the focal area. It should be less sensitive to fault irregularities and to stress or material small-scale inhomogeneities near the fault. The inversion for the composite moment tensor is more stable and more robust than the inversion for moment tensors of individual earthquakes.

The composite moment tensor is calculated using a joint inversion of earthquakes occurring in the same focal area. The earthquakes should display a similar focal mechanism associated with the same fault system. The basic principle of the method is to jointly invert observations gathered for

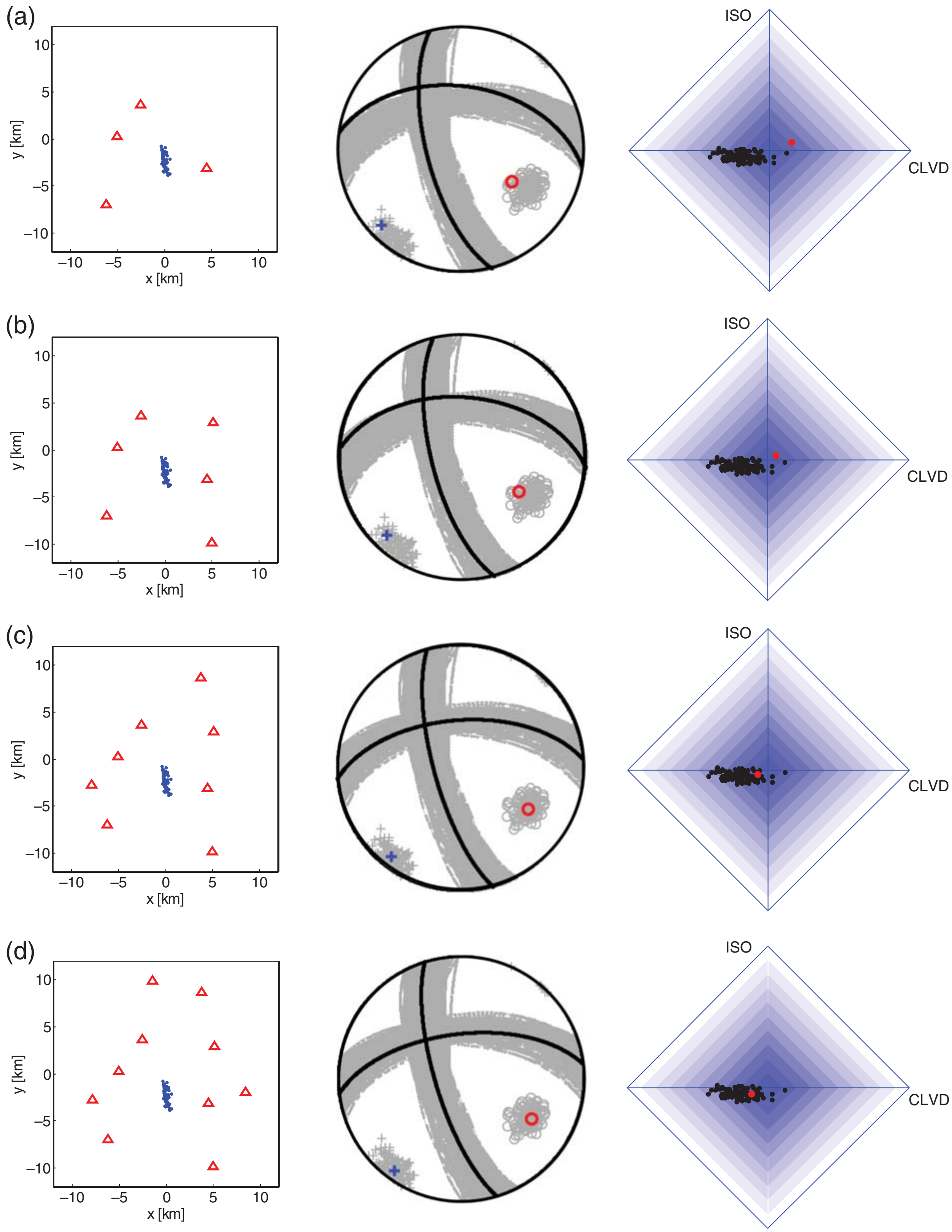

Figure 8. The composite moment tensor inversion of 111 selected earthquakes in the West Bohemia region using records at (a) 4, (b) 6, (c) 8, and (d) 10 stations. (left column) Locations of stations (red triangles) and epicenters of the earthquakes (blue dots). (middle column) Accurate focal mechanisms inverted using the standard moment tensor inversion of the *P*-wave amplitudes at a minimum of 18 stations (in gray) and the composite focal mechanism (in black). The P and T axes of the composite solution are marked by the red circle and blue plus sign. (right column) The diamond source-type plot (for its definition and basic properties, see Vavryčuk, 2015) showing the isotropic (ISO) and compensated linear vector dipole (CLVD) components of the accurate moment tensors (black dots) and of the composite solution (red dot). The DC percentage is color coded.

Table 1
Composite Moment Tensors

Stations	Strike (°)	Dip (°)	Rake (°)	DC (%)	CLVD (%)	ISO (%)
4	166.9	70.9	−42.3	82.1	15.1	2.7
6	165.5	70.1	−41.6	93.2	4.3	2.6
8	164.9	73.9	−33.7	88.4	−8.7	−2.8
10	163.7	74.1	−30.8	82.5	−13.3	−4.3
18	163.4	72.7	−32.7	78.2	−16.6	−5.2

"Stations" refers to the number of stations used in the inversion. The double-couple (DC), compensated linear vector dipole (CLVD), and isotropic (ISO) percentages were calculated according to formulas of Vavryčuk (2001).

many events for one single quantity. Consequently, the inversion for the composite moment tensor is more robust than that for individual moment tensors. The inversion can utilize amplitudes of the *P* and/or *S* waves or full waveforms and allows for determining the complete moment tensor including the non-DC components. Because the inversion is iterative with several linear steps, it is fast and applicable even to large datasets of multiple earthquakes.

The numerical tests show that the inversion is sensitive to noise in the data, number of stations used in the inversion, number of multiple earthquakes, scatter in their focal mechanisms, and number of outliers with a dissimilar focal mechanism. If many multiple earthquakes are recorded, the composite moment tensor can be determined from *P*-wave amplitudes measured at three stations only. The minimum number of earthquakes is about 100. For larger number of earthquakes and/or stations, the robustness and accuracy of the inversion increases. The accuracy can also be improved if the inversion is run in two steps. In the first step, the rms values are calculated for individual events. In the second step, the inversion is run after removing the outliers that do not fit the composite solution.

The waveform inversion is more robust than the amplitude inversion. The composite moment tensor can be calculated with a high accuracy even from waveforms of a few earthquakes. For example, instead of inverting for inaccurate moment tensors of five events recorded at three stations, we can invert for one accurate composite moment tensor using recordings at 15 stations. Obviously, the events should display reasonably similar moment tensors (except for scaling), and their locations must be different.

The method is particularly suitable for analyzing areas of permanent seismicity, aftershock sequences, earthquake swarms, or microseismicity, where observations of multiple events with uniform mechanisms produced by a single fault are available. If several faults are activated in the area, composite moment tensors associated with individual faults can be calculated. The method yields representative (averaged) moment tensors, including the non-DC components even when station configurations prevent inversion for the full moment tensors of individual earthquakes.

Data and Resources

The data for this article are available by contacting the author at vv@ig.cas.cz. The moment tensor decomposition was done and the diamond source-type plots in Figure 8 were prepared using the open access MATLAB package MT_DECOMPOSITION (http://www.ig.cas.cz/mt-decomposition, last accessed October 2015).

Acknowledgments

I thank Michel Bouchon and one anonymous reviewer for their helpful comments and Josef Horálek, Alena Boušková, and other colleagues of the West Bohemia Network (WEBNET) group for providing with the 2008 swarm data and for kind help with their preprocessing. The work was supported by the Grant Agency of the Czech Republic, Grant Numbers 210/12/1491 and 13-08971S.

References

Babuška, V., J. Plomerová, and T. Fischer (2007). Intraplate seismicity in the western Bohemian massif (central Europe): A possible correlation with a paleoplate junction, *J. Geodyn.* **44,** 149–159, doi: 10.1016/j.jog.2007.02.004.

Bouchaala, F., V. Vavryčuk, and T. Fischer (2013). Accuracy of the master-event and double-difference locations: Synthetic tests and application to seismicity in West Bohemia, Czech Republic, *J. Seismol.* **17,** no. 3, 841–859, doi: 10.1007/s10950-013-9357-4.

Čermáková, H., and J. Horálek (2015). The 2011 West Bohemia (Central Europe) earthquake swarm compared with the previous swarms of 2000 and 2008, *J. Seismol.* **19,** 899–913, doi: 10.1007/s10950-015-9502-3.

Červený, V. (2001). *Seismic Ray Theory*, Cambridge University Press, Cambridge, United Kingdom.

Ferreira, J. M., T. Oliveira, M. K. Takeya, and M. Assumpcao (1998). Superposition of local and regional stresses in northeast Brazil: Evidence from focal mechanisms around the Potiguar marginal basin, *Geophys. J. Int.* **134,** no. 2, 341–355.

Fischer, T., J. Horálek, P. Hrubcová, V. Vavryčuk, K. Bräuer, and H. Kämpf (2014). Intra-continental earthquake swarms in West Bohemia and Vogtland: A review, *Tectonophysics* **611,** 1–27, doi: 10.1016/j.tecto.2013.11.001.

Fischer, T., J. Horálek, J. Michálek, and A. Boušková (2010). The 2008 West Bohemia earthquake swarm in the light of the WEBNET network, *J. Seismol.* **14,** 665–682.

Fojtíková, L., and J. Zahradník (2014). A new strategy for weak events in sparse networks: The first-motion polarity solutions constrained by single-station waveform inversion, *Seismol. Res. Lett.* **85,** no. 6, 1265–1274, doi: 10.1785/0220140072.

Godano, M., A. Deschamps, S. Lambotte, H. Lyon-Caen, P. Bernard, and F. Pacchiani (2014). Focal mechanisms of earthquake multiplets in the western part of the Corinth rift (Greece): Influence of the velocity model and constraints on the geometry of the active faults, *Geophys. J. Int.* **197,** no. 3, 1660–1680, doi: 10.1093/gji/ggu059.

Got, J. L., J. Frechet, and F. W. Klein (1994). Deep fault plane geometry inferred from multiplet relative relocation beneath the south flank of Kilauea, *J. Geophys. Res.* **99,** no. B8, 15,375–15,386.

Julian, B. R., A. D. Miller, and G. R. Foulger (1998). Non-double-couple earthquakes. 1. Theory, *Rev. Geophys.* **36,** 525–549.

Li, L., Q.-F. Chen, F. Niu, and J. Su (2011). Deep slip rates along the Longmen Shan fault zone estimated from repeating microearthquakes, *J. Geophys. Res.* **116,** no. B09310, doi: 10.1029/2011JB008406.

Menke, W. (1989). *Geophysical Data Analysis: Discrete Inverse Theory*, Academic Press, New York, New York.

Miller, A. D., G. R. Foulger, and B. R. Julian (1998). Non-double-couple earthquakes. 2. Observations, *Rev. Geophys.* **36,** 551–568.

Myhill, R., D. McKenzie, and K. Priestley (2011). The distribution of earthquake multiplets beneath the southwest Pacific, *Earth Planet. Sci. Lett.* **301,** 87–97.

Rubin, A. M., D. Gillard, and J.-L. Got (1998). A reinterpretation of seismicity associated with the January 1983 dike intrusion at Kilauea Volcano, Hawaii, *J. Geophys. Res.* **103,** no. B5, 10,003–10,015.

Rutledge, J. T., and W. S. Phillips (2003). Hydraulic stimulation of natural fractures as revealed by induced microearthquakes, Carthage Cotton Valley gas field, east Texas, *Geophysics* **68,** no. 2, 441–452.

Rutledge, J. T., W. S. Phillips, and B. K. Schuessler (1998). Reservoir characterization using oil-production-induced microseismicity, Clinton County, Kentucky, *Tectonophysics* **289,** nos. 1/3, 129–152.

Sato, T., J. Kasahara, T. Taymaz, M. Ito, A. Kamimura, T. Hayakawa, and O. Tan (2004). A study of microearthquake seismicity and focal mechanisms within the Sea of Marmara (NW Turkey) using ocean bottom seismometers (OBSs), *Tectonophysics* **391,** nos. 1/4, 303–314.

Scarfi, L., H. Langer, and S. Gresta (2003). High-precision relative locations of two microearthquake clusters in southeastern Sicily, Italy, *Bull. Seismol. Soc. Am.* **93,** no. 4, 1479–1497.

Schaff, D. P., and P. G. Richards (2011). On finding and using repeating seismic events in and near China, *J. Geophys. Res.* **116,** no. B03309, doi: 10.1029/2010JB007895.

Shearer, P. M., J. L. Hardebeck, L. Astiz, and K. B. Richards-Dinger (2003). Analysis of similar event clusters in aftershocks of the 1994 Northridge, California, earthquake, *J. Geophys. Res.* **108,** no. B1, doi: 10.1029/2001JB000685.

Šílený, J. (2009). Resolution of non-double-couple mechanisms: Simulation of hypocenter mislocation and velocity structure mismodeling, *Bull. Seismol. Soc. Am.* **99,** no. 4, 2265–2272.

Stierle, E., M. Bohnhoff, and V. Vavryčuk (2014). Resolution of non-double-couple components in the seismic moment tensor using regional networks—II. Application to aftershocks of the 1999 M_w 7.4 Izmit earthquake, *Geophys. J. Int.* **196,** no. 3, 1878–1888, doi: 10.1093/gji/ggt503.

Stierle, E., V. Vavryčuk, J. Šílený, and M. Bohnhoff (2014). Resolution of non-double-couple components in the seismic moment tensor using regional networks—1: A synthetic case study, *Geophys. J. Int.* **196,** no. 3, 1869–1877, doi: 10.1093/gji/ggt502.

Vavryčuk, V. (2001). Inversion for parameters of tensile earthquakes, *J. Geophys. Res.* **106,** no. B8, 16,339–16,355, doi: 10.1029/2001JB000372.

Vavryčuk, V. (2002). Non-double-couple earthquakes of January 1997 in West Bohemia, Czech Republic: Evidence of tensile faulting, *Geophys. J. Int.* **149,** no. 2, 364–373, doi: 10.1046/j.1365-246X.2002.01654.x.

Vavryčuk, V. (2011a). Principal earthquakes: Theory and observations for the 2008 West Bohemia swarm, *Earth Planet. Sci. Lett.* **305,** nos. 3/4, 290–296, doi: 10.1016/j.epsl.2011.03.002.

Vavryčuk, V. (2011b). Tensile earthquakes: Theory, modeling, and inversion, *J. Geophys. Res.* **116,** no. B12, doi: 10.1029/2011JB008770.

Vavryčuk, V. (2015). Moment tensor decompositions revisited, *J. Seismol.* **19,** no. 1, 231–252, doi: 10.1007/s10950-014-9463-y.

Vavryčuk, V., and S. G. Kim (2014). Nonisotropic radiation of the 2013 North Korean nuclear explosion, *Geophys. Res. Lett.* **41,** doi: 10.1002/2014GL061265.

Vavryčuk, V., F. Bouchaala, and T. Fischer (2013). High-resolution fault image from accurate locations and focal mechanisms of the 2008 swarm earthquakes in West Bohemia, Czech Republic, *Tectonophysics* **590,** 189–195, doi: 10.1016/j.tecto.2013.01.025.

Zahradník, J., and S. Custodio (2012). Moment tensor resolvability: Application to southwest Iberia, *Bull. Seismol. Soc. Am.* **102,** no. 3, 1235–1254.

Institute of Geophysics
The Czech Academy of Sciences
Boční II/1401
141 00 Prague
Czech Republic
vv@ig.cas.cz

Manuscript received 29 September 2015;
Published Online 10 November 2015